ARTICLES SCIENCE CHINA Materials

mater.scichina.com link.springer.com

Published online 16 March 2017 | doi: 10.1007/s40843-017-9019-4
Sci China Mater 2017, 60(4): 352–360

Monolayer MoS_2 decorated Cu_7S_4-Au nanocatalysts for sensitive and selective detection of mercury(II)

Jiabin Cui, Suying Xu and Leyu Wang*

ABSTRACT Sensitive and selective detection of Hg(II) contamination is of great importance with concern of public health. Herein, we successfully fabricated monolayer MoS_2 (S-MoS_2) decorated Cu_7S_4-Au (Cu_7S_4-Au@S-MoS_2) nanocomposite modified electrode for the sensitive and selective detection of Hg(II) via anodic stripping voltammetric technique. Due to the excellent electrocatalytic reduction performance arisen from the abundant active edge sites of small monolayer MoS_2 and good affinity of Au toward Hg, the current method displayed high sensitivity (LOD = 190 nmol L^{-1}) and enhanced selectivity. As control, nanostructures including Cu_7S_4-Au, Cu_7S_4@S-MoS_2 and Cu_7S_4-Au@M-MoS_2 (M: multilayer) were also investigated, but showed low response to Hg(II), suggesting that both Au domains and active edge sites of monolayer MoS_2 have crucial synergistic effects on the high-performance for recognition of Hg(II). Moreover, the developed method displays satisfied performance for the detection of Hg(II) in real samples, which indicates its potentials in practical applications.

Keywords: Cu_7S_4-Au nanocatalysts, MoS_2, square wave anodic stripping voltammetry, mercury(II)

INTRODUCTION

Heavy metal ion contamination in water and soil, especially mercury, has been considered as one of the most severe threats to public health [1–7]. It is known that mercury is non-degradable and could be further accumulated along the food chain [8]. Even exposure to low level of mercury would cause severe damage to human organs such as kidney and nervous system [9]. Thus, it has a caused worldwide concerns for careful control of the mercury release and close monitoring of mercury level in environment and food process chains. To date, many kinds of sensing platform have been developed for detection of trace Hg(II) including conventional strategies like inductively coupled plasma mass spectrometry [10], atomic absorption spectrometry [11], colorimetry [12–14] and fluorometry [9,15–26]. Still, there is a growing demand for exploration of reliable, efficient but also cost-effective and portable methods. The electrochemical method is characterized by facile preparation, low-cost, miniaturization and portability [27,28]. In addition, there are many different electrochemical strategies that could increase the sensitivity as well as the selectivity. With regard to the detection of heavy metals, the stripping voltammetry method is particularly intriguing for trace amount of analyte given the unique properties of preconcentration of analytes [29]. Hence, great efforts were devoted to electrochemical sensor for Hg(II) [30–32]. For example, Fan's group constructed a sensitive electrochemical biosensor for detection of Hg(II) by using a thymine-rich, mercury-specific oligonucleotide modified gold nanoparticle probe [33]. The oligonucleotide could effectively capture free Hg(II) and the Au nanoparticles (NPs) were utilized to increase the loading density as well as reduce the steric hindrance of oligonucleotide, which then significantly enhance the responses. Zhao *et al.* [34] developed a photoelectrochemical biosensor for Hg(II) detection based on the exciton energy transfer between CdS quantum dots and Au NPs coupled with sensitization of rhodamine 123. The introduction of biomolecular recognition has achieved satisfied performance toward Hg(II) detection, however, in another aspect, it would induce stability issue. Alternatively, nanomaterial modified electrodes have demonstrated their great potentials for analyte sensing on account of the prevailing merits of the nanomaterials [32,35–43]. For instance, nanomaterial modified electrodes tend to own superb electroconductivity, increased mass transport, high surface absorption capability as well

State Key Laboratory of Chemical Resource Engineering, Beijing Key Laboratory of Environmentally Harmful Chemical Analysis, Beijing University of Chemical Technology (BUCT), Beijing 100029, China
* Corresponding author (email: lywang@mail.buct.edu.cn)

as sensitive signal responses originated from the unique properties of nanomaterials. In this regard, Gong *et al.* [44] constructed a Hg(II) on basis of a bimetallic Au-Pt nanoparticle/organic nanofibers. They reasoned that the three-dimensional nanofibers offer large effective surface area and the Au-Pt nanoparticles act as microelectrodes. Still, to construct a platform for sensitive detection of Hg(II) without compromise of the selectivity is always challenging.

Here in this work, we prepared a small monolayer MoS_2 decorated Cu_7S_4-Au nanocomposite (Cu_7S_4-Au@S-MoS_2, S-MoS_2 means single layered MoS_2) and employed it to modify glassy carbon electrode (GCE) for the sensitive and selective detection of Hg(II) via the square wave anodic stripping voltammetry (SWASV). The MoS_2 has been widely used as an alternative to platinum (Pt) for active hydrogen evolution from water due to its excellent catalytic performance and earth abundant reserves. The edges of layered MoS_2 structures have been experimentally [45–48] and theoretically [49,50] identified to be the active sites for catalysis. To increase the active edge sites and therefore enhance the electrocatalytic performance, the preparation of ultrasmall monolayer MoS_2 is highly desirable but greatly challenging. By utilizing Cu_7S_4 nanoparticles (NPs) [51–55] as templates, the ultrasmall Cu_7S_4@MoS_2 nanoframes and Cu_7S_4-Au@S-MoS_2 nanocomposites with abundant active MoS_2 edge sites have been successfully fabricated for efficient hydrogen evolution reaction [56,57], where the monolayer MoS_2 can reduce the proton into hydrogen. As shown in Fig. 1a, by taking advantage of the excellent reductive property of this MoS_2, Hg(II) could be reduced to Hg(0) and enriched through anodic stripping voltammetry, which, in a significant way, improves the sensitivity of this method. The results also indicate that the Au domains play a synergistic effect on the sensitive recognition of Hg(II) due to the good affinity of Au toward Hg(II). Furthermore, this method has demonstrated its wide adaptability for recognition of Hg(II) in real samples.

MATERIALS AND METHODS

Materials

Nafion (5%), 1-octadecene (ODE), $MoCl_5$, oleylamine (OAm), and commercial 20 wt.% Pt/C were all purchased from Alfa. Ethanol, hexane, chloroform, acetic acid (AA), isopropanol, $HAuCl_4{\cdot}4H_2O$, H_2SO_4 (98%), $HgCl_2$, $NaH_2PO_4{\cdot}2H_2O$, Na_2HPO_4, NaCl, $CdCl_2{\cdot}2.5H_2O$, $Pb(NO_3)_2$, $CuSO_4{\cdot}5H_2O$ and NH_4Cl were obtained from Beijing Chemical Reagent Company. Ketjen carbon (EC-300J) was purchased from River's Electric Co. Ltd. Sulfur was purchased from Xilong Chemical Co. Ltd. *N, N′*-dibutyldithiocarbamic acid (HS_2CNBut_2) was obtained from Pacific Ocean United Petro-Chemical Company, Ltd. All the reagents were of analytical grade and used as received without further purification.

Characterization

The characterization of the as-prepared nanomaterials was carried out on a JEM-1200EX (JEOL) transmission electron microscope (TEM) at 100 kV and a JEM-2100F high resolution TEM (HRTEM) at 200 kV. All the electrochemical tests were performed on an electrochemical workstation (CHI 660E, CH Instrument, Inc.).

Synthesis of Cu_7S_4 NPs

The Cu_7S_4 NPs were synthesized with a solvothermal strategy. Prior to the synthesis of Cu_7S_4 NPs, the $Cu(DT)_2$ precursor solution was prepared by mixing HS_2CNBut_2 (represented by DT, 30 mg) and $Cu(NO_3)_2{\cdot}3H_2O$ (0.1 mmol) in ethanol (1.0 mL). Then the as-prepared $Cu(DT)_2$ was added to a 50-mL three-necked flask containing the mixture of ODE (6.0 mL) and OAm (4.0 mL) at 205°C with nitrogen atmosphere and vigorous magnetic stirring. The temperature was kept at 190°C for 15 min before the solution was cooled naturally to room temperature and the Cu_7S_4 NPs were collected via centrifugation and stored in 1.0 mL of chloroform for later use.

Synthesis of Cu_7S_4@S-MoS_2 NPs

In brief, 4.0 mL of OAm, 6.0 mL of ODE and 1.0 mL of the as-synthesized Cu_7S_4 colloids were mixed in a 50-mL three-necked flask. After the temperature of the solution was raised to 310°C, 1 mL of OAm containing 0.008 mmol $MoCl_5$ and 0.016 mmol S was injected. Ten minutes later, the resultant solution was naturally cooled to room temperature and the as-prepared Cu_7S_4@S-MoS_2 NPs were collected.

Synthesis of Cu_7S_4-Au@S-MoS_2 NPs

For the fabrication of Cu_7S_4-Au@S-MoS_2, the temperature of the as-prepared Cu_7S_4@S-MoS_2 colloidal solution was cooled from 310°C to 190°C, and then the $HAuCl_4{\cdot}4H_2O$ (10 mg) in ethanol (1.0 mL) was injected. The temperature was kept at 160°C for 10 min, then the solution was cooled to room temperature naturally. The final products of Cu_7S_4-Au@S-MoS_2 NPs were then collected via centrifugation after washing with ethanol.

Synthesis of Cu_7S_4-Au@M-MoS_2 NPs

Similarly, the Cu_7S_4-Au@M-MoS_2 NPs (M: multilager) were prepared with the Cu_7S_4@M-MoS_2 NPs as seeds. These Cu_7S_4@M-MoS_2 NPs were synthesized via the similar protocol for Cu_7S_4@S-MoS_2 NPs but with different dosage of Mo (0.075 mmol) and S (0.125 mmol). Then, the solution of $HAuCl_4{\cdot}4H_2O$ (10 mg) in ethanol (1.0 mL) was injected into the flask containing the Cu_7S_4@M-MoS_2 colloids, and the temperature was maintained at 160°C for 10 min before the solution was naturally cooled to room temperature. Finally, the Cu_7S_4-Au@M-MoS_2 NPs were collected via centrifugation after washing with ethanol.

Synthesis of Cu_7S_4@Au heterostructures:

In brief, 4.0 mL of OAm, 6.0 mL of ODE and 1.0 mL of Cu_7S_4 colloids were mixed in a 50-mL three-necked flask. Thereafter, the temperature of the solution was rapidly raised to 180°C before the $HAuCl_4{\cdot}4H_2O$ (10 mg) in ethanol (1.0 mL) was injected. The temperature was dropped to and kept at 160°C for 10 min. Thereafter the resultant solution was finally cooled to 60°C. The addition of ethanol (30 mL) to the reaction mixture afforded a black product by centrifugation. The precipitations were then washed twice with hexane and precipitated with ethanol. Finally, the as-prepared Cu_7S_4@Au heterostructures were dispersed in 2 mL of chloroform and stored for later use.

Fabrication of electrodes

Prior to electrochemical detection, the working electrodes were modified with the nanocatalyst ink. The catalyst ink was prepared as follows. In brief, the as-prepared nanocatalysts were dispersed in 2.0 mL of hexane, and then 3.0 mL of hexane containing 2.0 mg of Ketjen carbon (EC-300J) was added. Thereafter, the mixture was sonicated for at least 1 h to make them thoroughly mixed before excess ethanol (10.0 mL) was added. Then the solid was collected by centrifugation (10,000 rpm for 10 min). The collected products were washed for further two times. The powder was then suspended in 40.0 mL of AA and treated at 70°C for 15 h to remove the surfactants on the nanocatalysts. The AA-treated nanocatalysts were collected with centrifugation (10,000 rpm for 10 min) and washed with water. Finally, the clean nanocatalysts were re-suspended in a mixture consisting of isopropanol (500 μL), water (500 μL), and Nafion (5%, 30 μL) to form a homogeneous nanocatalyst ink. This nanocatalyst ink was stored at 4°C for later electrochemical tests.

Electrochemical detection of mercury

For different nanocomposites, the electrochemical measurement setup was similar. In a typical case, the Cu_7S_4-Au@S-MoS_2 modified GCE was used as the working electrode with SWASV technique under optimized conditions with saturated calomel electrode (SCE) and carbon rod as the reference and counter electrode, respectively. For mercury deposition, the as-prepared Cu_7S_4-Au@S-MoS_2/GCE was dipped in 0.1 mol L^{-1} phosphate buffer solution (PBS, pH 5.0) containing a certain amount of Hg(II) and kept at −0.4 V for 200 s. The anodic stripping was performed from −0.6 to 0.6 V with the following parameters: frequency, 15 Hz; amplitude, 25 mV; increment potential, 4 mV. After each measurement, the as-prepared electrode was regenerated in a freshly stirred supporting electrolyte by desorption at 0.2 V for 60 s to remove the previous residual mercury from the electrode surface.

RESULTS AND DISCUSSION

Synthesis and characterization of nanocomposites

Fig. 1a shows the scheme for the electrochemical reduction of Hg(II) on the surface of Cu_7S_4-Au@S-MoS_2 nanocomposites. The TEM (Fig. 1b) and HRTEM (Fig. 1c) images clearly indicate the existence of Cu_7S_4 nanoplate, monolayer MoS_2 and Au domains. The lattice spacings of Cu_7S_4 and Au in the HRTEM image were determined to be 0.193 and 0.236 nm, corresponding well with (0160) plane of Cu_7S_4 (14.5 ± 1.1 nm, Fig. S1a) and (111) plane of Au (5.7 ± 1.6 nm, Fig. S1b), respectively. The monolayer-MoS_2 nanosheet on the surface of Cu_7S_4 is also clearly shown in the HRTEM image. For better comparison, the Cu_7S_4-Au,

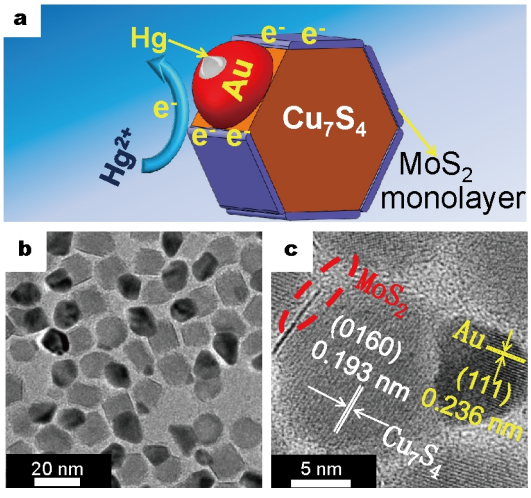

Figure 1 Schematic illustration for the mercury detection (a), TEM (b) and HRTEM (c) images of Cu_7S_4-Au@S-MoS_2 NPs.

Cu_7S_4@S-MoS_2 and Cu_7S_4-Au@M-MoS_2 (Fig. S2) nanostructures were also synthesized accordingly and characterized with TEM and HRTEM (Fig. S3). Initially, the cyclic voltammetry (CV) experiments were carried out to evaluate the electrochemical responses of the nanocomposite modified electrode. For bare GCE, there is no peak in the presence of 3 μmol L^{-1} Hg(II) (Fig. 2). While there is an oxidation peak at 0.06 V for Cu_7S_4-Au@S-MoS_2 nanocomposites modified GCE in the presence of Hg(II), which could be ascribed to the oxidation of Hg(0) to Hg(II).

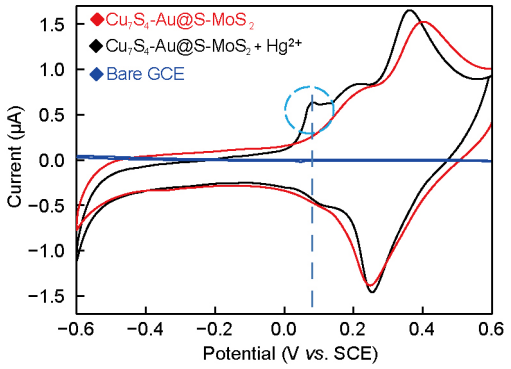

Figure 2 CV scans of Cu_7S_4-Au@S-MoS_2/GCE in the absence (red line) and presence of 3 μmol L^{-1} Hg(II) (black line).

Mercury detection

It is known that stripping voltammetric technique holds great advantages, particularly for electrochemical detection of trace metals. Here, the SWASV mode was selected for the detection of Hg(II). Prior to investigating its capability for the determination of Hg(II), a series of experimental parameters were optimized. Initially, we found the types of buffer solution have a great impact on the stripping signals. As indicated in Fig. 3a, the phosphate buffer gives the best signals as compared to the NH_4Cl-NH_3·H_2O and NaOAc-HOAc systems when fixing all the pH value of the buffer solutions at around 5.0. With respect to the pH effect, the maximal peak current appears at pH 5.0 (Fig. 3b). We assumed that too acidic pH condition may result in competitive reduction of protons, whereas too alkali condition would lead to the formation of metal hydroxides. Additionally, the deposition potential as well as the deposition time was also optimized and a deposition potential of −0.4 V with a duration time of 200 s gave the best performance for the Hg stripping responses (Fig. 3c, d).

Under the optimized condition, Cu_7S_4-Au@S-MoS_2/GCE was utilized for the determination of Hg(II). Specifically, the Hg(II) was firstly reduced to Hg(0) and deposited at the working electrode under optimized −0.4 V for 200 s and then anodic stripping from −0.6 to 0.6 V was performed,

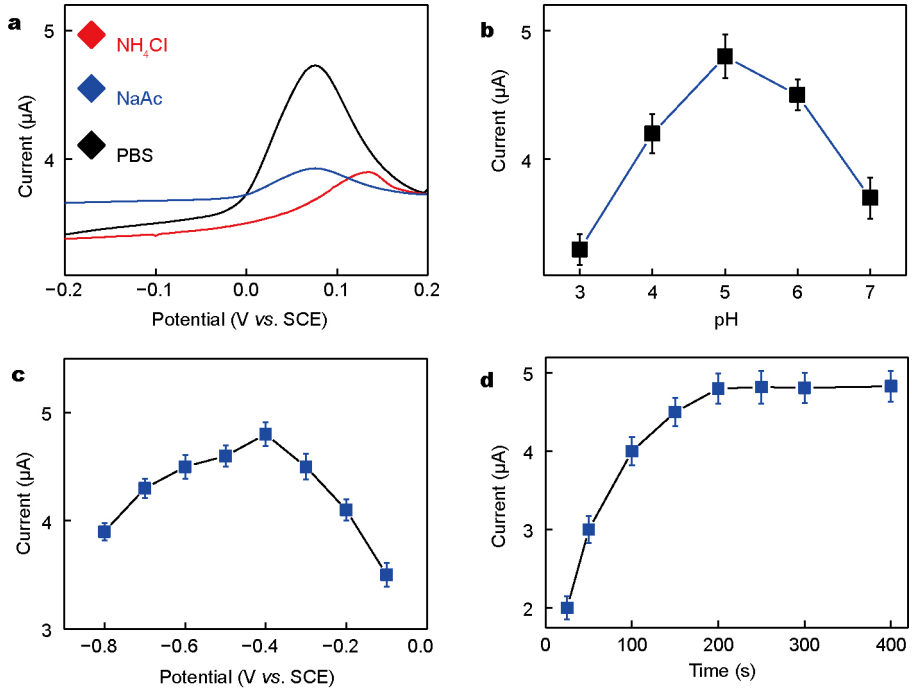

Figure 3 Effects of buffer solutions (a), pH conditions (b), deposition potentials (c) and deposition duration (d) on the stripping signals of Hg(II). The concentration of Hg(II) is 1.0 μmol L^{-1}.

where the anodic stripping signal was proportional to the concentration of Hg(II) in solution and accordingly used to monitor its concentration. Thus, a series of solutions with different concentrations of Hg(II) were applied. A well-defined stripping peak at the potential of ~0.06 V *vs.* SCE appeared and increased step by step as shown in Fig. 4a. In addition, a good linear fitting of peak current difference ($\Delta I = I - I_0$) *vs.* Hg(II) concentration was also obtained (inset in Fig. 4a) with a limit of detection (LOD) of 190 nmol L^{-1} (LOD = $3\sigma/K$). This method is comparable to or even more sensitive than some of the reported methods for Hg(II) detection (Table S1). Herein I and I_0 represent the current in the presence and absence of Hg(II), respectively. The σ is the standard deviation of the blank measurement (n = 6), and K is the slope of the linear fitting curve. For comparison, its counterparts including Cu_7S_4-Au, Cu_7S_4@S-MoS_2, and Cu_7S_4-Au@M-MoS_2 nanocomposites were also investigated for their responses toward Hg(II). Under the identical conditions, it was found that much less SWASV responses were observed for Cu_7S_4-Au@M-MoS_2/GCE (Fig. S4) with an LOD of 628 nmol L^{-1}. These results unambiguously indicate that the monolayer MoS_2 is more sensitive to Hg(II) than the multilayer MoS_2, which can be attributed to the increased active sites of monolayer MoS_2. As aforementioned, the layer edges of MoS_2 have been experimentally and theoretically identified to be the electrochemical active sites [45,46]. As a result, the electrochemical response of monolayer MoS_2 was more sensitive than that of multilayer MoS_2. Meanwhile, for nanocomposites either in the absence of Au (Cu_7S_4@S-MoS_2) or MoS_2 component (Cu_7S_4-Au), almost negligible response toward Hg(II) was obtained (Fig. S5). To compare their sensitivity directly, their electrochemical responses under the same concentration (3.68 μmol L^{-1}) of Hg(II) are shown in Fig. 4b.

Clearly, the type of the nanocomposites plays a crucial role in the recognition of Hg(II). It is found that both MoS_2 and Au components have synergistic effects on the sensitive sensing of Hg(II). To further investigate the synergistic effects, the Cu_7S_4@S-MoS_2 and Cu_7S_4-Au were physically mixed and then pasted onto the GCE. As shown in Fig. S6, the as-prepared GCE shows a very weak response to Hg(II) even though the concentration of Hg(II) is up to 3.68 μmol L^{-1}. These results suggest that the Au and MoS_2 should directly or indirectly contact by means of Cu_7S_4 via forming a heterostructure [58–60]. Otherwise, the synergistic effects cannot be obtained. In a word, the high-performance for Hg(II) recognition can be attributed to the synergistic effects of Au domains and monolayer MoS_2. Moreover, the number of MoS_2 layers also affects sensitivity towards Hg(II). As discussed in previous work, the MoS_2 active sites display significant enhancement of catalytic ability toward electrochemical hydrogen evolution reaction [54]. Thus, we assume that the reductive properties of monolayer MoS_2 as well as high affinity of Au toward mercury account for the high sensitivity of Cu_7S_4-Au@S-MoS_2 nanocomposites.

Furthermore, to evaluate the selectivity of the developed method, the SWASV responses of the Cu_7S_4-Au@S-MoS_2/GCE toward Hg(II) in the coexistence of different cations were performed, since different metal ions often present together in real samples. Here, the possible interferences such as Cd(II), Pb(II), Cu(II) were examined. The SWASV responses of mercury in the presence of 10-fold concentration (10 μmol L^{-1}) of the interfering metal ions with respect to Hg(II) (1.0 μmol L^{-1}) are displayed in Fig. 5. Though at the experimental conditions, the interfering metal ion could be co-deposited and stripped off, the stripping potentials were different and

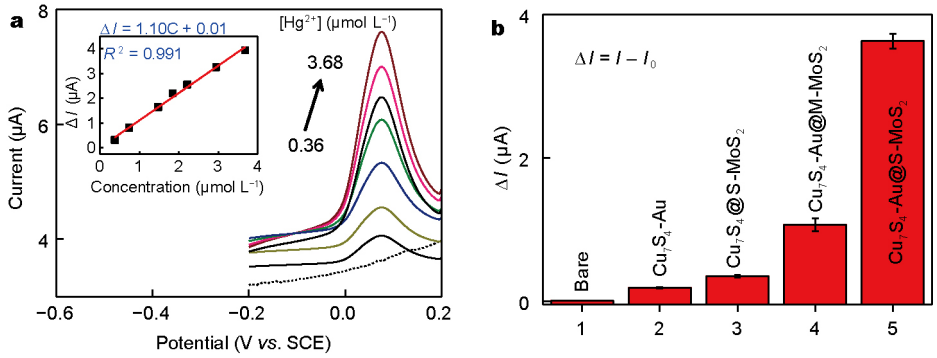

Figure 4 (a) Typical SWASV responses for the Cu_7S_4-Au@S-MoS_2/GCE in the presence of Hg(II) under different concentrations. Inset of (a) is the corresponding linear fitting curve; (b) comparison of sensitivities of GCE (1), Cu_7S_4-Au/GCE (2), Cu_7S_4@S-MoS_2/GCE (3), Cu_7S_4-Au@M-MoS_2/GCE (4), and Cu_7S_4-Au@S-MoS_2/GCE (5) for SWASV detection of mercury (3.68 μmol L^{-1}). $\Delta I = I - I_0$, I and I_0 represent the current in the presence and absence of Hg(II), respectively.

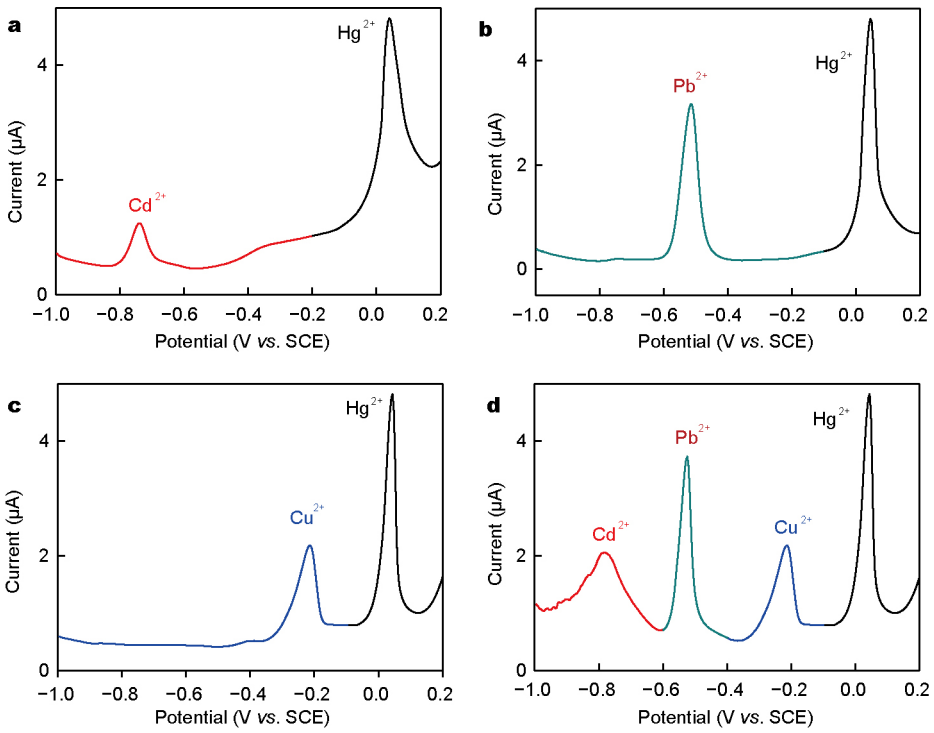

Figure 5 Stripping voltammograms in the presence of potential interferences: Cd^{2+}+ Hg(II) (a); Pb^{2+}+ Hg(II) (b); Cu^{2+}+ Hg(II) (c) and Cd^{2+}+ Pb^{2+}+ Cu^{2+}+ Hg(II) (d) in PBS (0.02 mol L^{-1}, pH 5). Concentration of Hg(II) is 1.0 μmol L^{-1} and that of other cation is 10 μmol L^{-1}.

Table 1 Effects of different metal ions on the electrochemical stripping signals of Hg(II) with Cu_7S_4-Au@S-MoS_2/GCE

Metal ions[a)]	Signals at 0.04 V (μA)	Contribution (%)[b)]
Hg(II)	4.789	0
Hg(II), Cd(II)	4.824	+0.73
Hg(II), Pb(II)	4.801	+0.25
Hg(II), Cu(II)	4.816	+0.56
Hg(II), Cd(II), Pb(II),Cu(II)	4.806	+0.35

a) 1.0 μmol L^{-1} of Hg(II) and 10 μmol L^{-1} of Cd(II), Pb(II) and Cu(II). b) Contribution refers to the effect of the interfering cations on the signals of Hg(II).

could be well-recognized from each other. These results indicate that the proposed method can differentiate multiple metal ions in one time. Moreover, when carefully comparing the electrochemical stripping signals of mercury in the absence and presence of interferences, one can easily find that the stripping peak current of 1.0 μmol L^{-1} Hg(II) varies slightly (Table 1) in comparison with that in the presence of only Hg(II) (Fig. S7), implying that these metal ions have negligible effects on the detection of Hg(II). We assume that such good selectivity is ascribed to the excellence electrochemical properties of the Cu_7S_4-Au@S-MoS_2 nanocomposites.

Practical applications

In another aspect, the proposed method was also employed for the recognition of Hg(II) in real water samples to further demonstrate its practicality. Three different lake water samples were collected from Beijing, Tianjin and Shijiazhuang, respectively and treated with a standard 0.45 μm filter. All the water samples were spiked with 2.0 μmol L^{-1} Hg(II) and then analysed with the developed protocols. The results, summarized in Table 2, demonstrate that the proposed method achieved satisfied performance with high accuracy and good reproducibility, implying its great promising in practical applications.

Table 2 Analytical results for the detection of Hg(II) in real water samples

Sample	Concentration (μmol L^{-1})		Recovery (%)
	Taken	Found (Mean, $n = 6$) [a]	
Water 1	2.0	2.01 ± 0.13	100.5 ± 5.5
Water 2	2.0	2.03 ± 0.07	102.0 ± 3.4
Water 3	2.0	1.96 ± 0.15	98.0 ± 7.6

a) n is the number of repetitive measurements.

CONCLUSION

Here, a facile platform for sensitive and selective analysis of Hg(II) was constructed. The Cu_7S_4-Au@S-MoS_2 nanocomposites were prepared and utilized for the modification of electrode. Both Au domains and single-layered MoS_2 have crucial synergistic effects on its high-performance for recognition of Hg(II). The results imply that the proposed method can not only measure Hg(II) in a highly sensitive way, but also recognize multiple coexisting metal ions in one time. Additionally, this method displays satisfied performance for the detection of Hg(II) in real samples, which indicates its great potentials in practical applications.

Received 5 February 2017; accepted 7 March 2017; published online 16 March 2017

1 Huber J, Leopold K. Nanomaterial-based strategies for enhanced mercury trace analysis in environmental and drinking waters. TrAC Trends Anal Chem, 2016, 80: 280–292
2 Chen J, Zhou S, Wen J. Disposable strip biosensor for visual detection of Hg^{2+} based on Hg^{2+}-triggered toehold binding and exonuclease III-assisted signal amplification. Anal Chem, 2014, 86: 3108–3114
3 Yuan C, Zhang K, Zhang Z, *et al.* Highly selective and sensitive detection of mercuric ion based on a visual fluorescence method. Anal Chem, 2012, 84: 9792–9801
4 Yuan C, Liu B, Liu F, *et al.* Fluorescence "turn on" detection of mercuric ion based on bis(dithiocarbamato)copper(II) complex functionalized carbon nanodots. Anal Chem, 2014, 86: 1123–1130
5 Duan J, Zhan J. Recent developments on nanomaterials-based optical sensors for Hg^{2+} detection. Sci China Mater, 2015, 58: 223–240
6 Du Y, Liu R, Liu B, *et al.* Surface-enhanced raman scattering chip for femtomolar detection of mercuric ion (II) by ligand exchange. Anal Chem, 2013, 85: 3160–3165
7 Han G, Liu R, Han MY, *et al.* Label-free surface-enhanced raman scattering imaging to monitor the metabolism of antitumor drug 6-mercaptopurine in living cells. Anal Chem, 2014, 86: 11503–11507
8 Duong TQ, Kim JS. Fluoro- and chromogenic chemodosimeters for heavy metal ion detection in solution and biospecimens. Chem Rev, 2010, 110: 6280–6301
9 Ruan YB, Xie J. Unexpected highly selective fluorescence 'turn-on' and ratiometric detection of Hg^{2+} based on fluorescein platform. Tetrahedron, 2011, 67: 8717–8723
10 Ma S, He M, Chen B, *et al.* Magnetic solid phase extraction coupled with inductively coupled plasma mass spectrometry for the speciation of mercury in environmental water and human hair samples. Talanta, 2016, 146: 93–99
11 Türker AR, Çabuk D, Yalçınkaya Ö. Preconcentration, speciation, and determination of mercury by solid phase extraction with cold vapor atomic absorption spectrometry. Anal Lett, 2013, 46: 1155–1170
12 Li T, Dong S, Wang E. Label-free colorimetric detection of aqueous mercury ion (Hg^{2+}) using Hg^{2+}-modulated G-quadruplex-based DNAzymes. Anal Chem, 2009, 81: 2144–2149
13 Wang H, Li Y, Xu S, *et al.* Rhodamine-based highly sensitive colorimetric off-on fluorescent chemosensor for Hg^{2+} in aqueous solution and for live cell imaging. Org Biomol Chem, 2011, 9: 2850–2855
14 Cui J, An M, Wang L. Nanocomposite-based rapid, visual, and selective luminescence turn-on assay for Hg^{2+} sensing in aqueous media. Talanta, 2013, 115: 512–517
15 Jeong Y, Yoon J. Recent progress on fluorescent chemosensors for metal ions. Inorg Chim Acta, 2012, 381: 2–14
16 Zou Q, Zou L, Tian H. Detection and adsorption of Hg^{2+} by new mesoporous silica and membrane material grafted with a chemodosimeter. J Mater Chem, 2011, 21: 14441–14447
17 Jiang T, Guo D, Wang Q, *et al.* Developing a genetically encoded green fluorescent protein mutant for sensitive light-up fluorescent sensing and cellular imaging of Hg(II). Anal Chim Acta, 2015, 876: 77–82
18 Zhang JF, Kim JS. Small-molecule fluorescent chemosensors for Hg^{2+} ion. Anal Sci, 2009, 25: 1271–1281
19 Yoon S, Miller EW, He Q, *et al.* A bright and specific fluorescent sensor for mercury in water, cells, and tissue. Angew Chem Int Ed, 2007, 46: 6658–6661
20 Yoon S, Albers AE, Wong AP, *et al.* Screening mercury levels in fish with a selective fluorescent chemosensor. J Am Chem Soc, 2005, 127: 16030–16031
21 Tsukamoto K, Shinohara Y, Iwasaki S, *et al.* A coumarin-based fluorescent probe for Hg^{2+} and Ag^{+} with an N'-acetylthioureido group as a fluorescence switch. Chem Commun, 2011, 47: 5073–5075
22 Liu F, Ding C, Jin M, *et al.* A highly selective two-photon fluorescent probe for the determination of mercury ions. Analyst, 2015, 140: 3285–3289
23 Ding C, Zhu A, Tian Y. Functional surface engineering of C-dots for fluorescent biosensing and *in vivo* bioimaging. Acc Chem Res, 2014, 47: 20–30
24 Shi Y, Wang W, Zhan J. A positively charged silver nanowire membrane for rapid on-site swabbing extraction and detection of trace inorganic explosives using a portable Raman spectrometer. Nano Res, 2016, 9: 2487–2497
25 Li Z, Zhao Q, Fan W, *et al.* Porous SnO_2 nanospheres as sensitive gas sensors for volatile organic compounds detection. Nanoscale,

2011, 3: 1646–1652
26 Fan Y, Liu Z, Wang L, *et al.* Synthesis of starch-stabilized Ag nanoparticles and Hg^{2+} recognition in aqueous media. Nanoscale Res Lett, 2009, 4: 1230–1235
27 Li X, Wen H, Fu Q, *et al.* Morphology-dependent NiO modified glassy carbon electrode surface for lead(II) and cadmium(II) detection. Appl Surface Sci, 2016, 363: 7–12
28 Gao C, Yu XY, Xiong SQ, *et al.* Electrochemical detection of arsenic(III) completely free from noble metal: Fe_3O_4 microspheres-room temperature ionic liquid composite showing better performance than gold. Anal Chem, 2013, 85: 2673–2680
29 Wei Y, Yang R, Yu XY, *et al.* Stripping voltammetry study of ultra-trace toxic metal ions on highly selectively adsorptive porous magnesium oxide nanoflowers. Analyst, 2012, 137: 2183–2191
30 Bhanjana G, Dilbaghi N, Kumar R, *et al.* Zinc oxide quantum dots as efficient electron mediator for ultrasensitive and selective electrochemical sensing of mercury. Electrochim Acta, 2015, 178: 361–367
31 Tavakoli MM, Tayyebi A, Simchi A, *et al.* Physicochemical properties of hybrid graphene–lead sulfide quantum dots prepared by supercritical ethanol. J Nanopart Res, 2015, 17: 9
32 Gao C, Huang XJ. Voltammetric determination of mercury(II). TrAC Trends Anal Chem, 2013, 51: 1–12
33 Zhu Z, Su Y, Li J, *et al.* Highly sensitive electrochemical sensor for mercury(II) ions by using a mercury-specific oligonucleotide probe and gold nanoparticle-based amplification. Anal Chem, 2009, 81: 7660–7666
34 Zhao M, Fan GC, Chen JJ, *et al.* Highly sensitive and selective photoelectrochemical biosensor for Hg^{2+} detection based on dual signal amplification by exciton energy transfer coupled with sensitization effect. Anal Chem, 2015, 87: 12340–12347
35 Abollino O, Giacomino A, Malandrino M, *et al.* Determination of mercury by anodic stripping voltammetry with a gold nanoparticle-modified glassy carbon electrode. Electroanalysis, 2008, 20: 75–83
36 Martín-Yerga D, González-García MB, Costa-García A. Electrochemical determination of mercury: a review. Talanta, 2013, 116: 1091–1104
37 Li M, Gou H, Al-Ogaidi I, *et al.* Nanostructured sensors for detection of heavy metals: a review. ACS Sustain Chem Eng, 2013, 1: 713–723
38 Aragay G, Pons J, Merkoçi A. Recent trends in macro-, micro-, and nanomaterial-based tools and strategies for heavy-metal detection. Chem Rev, 2011, 111: 3433–3458
39 Aragay G, Merkoçi A. Nanomaterials application in electrochemical detection of heavy metals. Electrochim Acta, 2012, 84: 49–61
40 Wang Y, Liu L, Li M, *et al.* Multifunctional carbon nanotubes for direct electrochemistry of glucose oxidase and glucose bioassay. Biosens Bioelectron, 2011, 30: 107–111
41 Song Q, Li M, Huang L, *et al.* Bifunctional polydopamine@Fe_3O_4 core–shell nanoparticles for electrochemical determination of lead(II) and cadmium(II). Anal Chim Acta, 2013, 787: 64–70
42 Bai F, Wang D, Huo Z, *et al.* A versatile bottom-up assembly approach to colloidal spheres from nanocrystals. Angew Chem Int Ed, 2007, 46: 6650–6653
43 Wu Y, Wang D, Li Y. Understanding of the major reactions in solution synthesis of functional nanomaterials. Sci China Mater, 2016, 59: 938–996
44 Gong J, Zhou T, Song D, *et al.* Stripping voltammetric detection of mercury(II) based on a bimetallic Au–Pt inorganic–organic hybrid nanocomposite modified glassy carbon electrode. Anal Chem, 2010, 82: 567–573
45 Jaramillo TF, Jørgensen KP, Bonde J, *et al.* Identification of active edge sites for electrochemical H_2 evolution from MoS_2 nanocatalysts. Science, 2007, 317: 100–102
46 Karunadasa HI, Montalvo E, Sun Y, *et al.* A molecular MoS_2 edge site mimic for catalytic hydrogen generation. Science, 2012, 335: 698–702
47 Yang X, Li Q, Hu G, *et al.* Controlled synthesis of high-quality crystals of monolayer MoS_2 for nanoelectronic device application. Sci China Mater, 2016, 59: 182–190
48 Yang Y, Xu X, Wang X. Synthesis of Mo-based nanostructures from organic-inorganic hybrid with enhanced electrochemical for water splitting. Sci China Mater, 2015, 58: 775–784
49 Hinnemann B, Moses PG, Bonde J, *et al.* Biomimetic hydrogen evolution: MoS_2 nanoparticles as catalyst for hydrogen evolution. J Am Chem Soc, 2005, 127: 5308–5309
50 Tsai C, Abild-Pedersen F, Nørskov JK. Tuning the MoS_2 edge-site activity for hydrogen evolution via support interactions. Nano Lett, 2014, 14: 1381–1387
51 Cui J, Xu S, Guo C, *et al.* Highly efficient photothermal semiconductor nanocomposites for photothermal imaging of latent fingerprints. Anal Chem, 2015, 87: 11592–11598
52 Cui J, Li Y, Liu L, *et al.* Near-infrared plasmonic-enhanced solar energy harvest for highly efficient photocatalytic reactions. Nano Lett, 2015, 15: 6295–6301
53 Huang S, Liu J, He Q, *et al.* Smart $Cu_{1.75}S$ nanocapsules with high and stable photothermal efficiency for NIR photo-triggered drug release. Nano Res, 2015, 8: 4038–4047
54 Cui J, Jiang R, Xu S, *et al.* Cu_7S_4 nanosuperlattices with greatly enhanced photothermal efficiency. Small, 2015, 11: 4183–4190
55 Li Y, Bai X, Xu M, *et al.* Photothermo-responsive Cu_7S_4@polymer nanocarriers with small sizes and high efficiency for controlled chemo/photothermo therapy. Sci China Mater, 2016, 59: 254–264
56 Xu J, Cui J, Guo C, *et al.* Ultrasmall Cu_7S_4@MoS_2 hetero-nanoframes with abundant active edge sites for ultrahigh-performance hydrogen evolution. Angew Chem Int Ed, 2016, 55: 6502–6505
57 Cui J, Jiang R, Lu W, *et al.* Plasmon-enhanced photoelectrical hydrogen evolution on monolayer MoS_2 decorated $Cu_{1.75}S$-Au nanocrystals. Small, 2017, 13: 1602235–1602241
58 Cravanzola S, Muscuso L, Cesano F, *et al.* MoS_2 nanoparticles decorating titanate-nanotube surfaces: combined microscopy, spectroscopy, and catalytic studies. Langmuir, 2015, 31: 5469–5478
59 Su S, Zhang C, Yuwen L, *et al.* Uniform Au@Pt core–shell nanodendrites supported on molybdenum disulfide nanosheets for the methanol oxidation reaction. Nanoscale, 2016, 8: 602–608
60 Zhang J, Wang T, Pohl D, *et al.* Interface engineering of MoS_2/Ni_3S_2 heterostructures for highly enhanced electrochemical overall-water-splitting activity. Angew Chem Int Ed, 2016, 55: 6702–6707

Acknowledgments This work was supported by the National Natural Science Foundation of China (21475007 and 21675009) and the Fundamental Research Funds for Central Universities (buctrc201507 and buctrc201608). We also thank the support from the "Public Hatching Platform for Recruited Talents of BUCT".

Author contributions Wang L proposed and guided the project. Cui J and Xu S designed and performed the experiments. Cui J, Xu S and Wang L analzed and discussed the experimental results, and drafted the manuscript. All the authors checked the manuscript.

Conflict of interest The authors have declared that no competing interest exists.

Supplementary information Supporting data are available in the online version of this paper.

Jiabin Cui currently is a PhD candidate in BUCT. His PhD project is focused on the design and fabrication of chalcogenide nanostructures for photoelctrical catalysis, sensing and bioimaging.

Leyu Wang is a professor of chemistry at BUCT. He received his PhD in chemistry from Tsinghua University with Prof. Yadong Li in 2007. Then he joined Prof. Yu Huang's group at the University of California at Los Angeles (UCLA) as a postdoctoral researcher from 2007–2009. He moved to BUCT's Chemistry Department in October 2009. His research interests span from the controlled synthesis of upconversion luminescence nanoparticles (UCNPs), localized surface plasmon resonance (LSPR) near-infrared (NIR) semiconductor NPs, magnetic nanomaterials, metal-semiconductor heteronanostructures, and molecularly imprinted polymers (MIPs) nanomaterials to the applications including electrocatalysis, artificial photosynthesis, biochemical sensing, multimodal imaging, drug/gene delivery and photothermo/chemo therapy.

单层MoS_2修饰Cu_7S_4-Au纳米结构用于汞的灵敏选择性检测

崔家斌, 许苏英, 汪乐余*

摘要 汞的灵敏选择性检测对于人类的公共安全至关重要. 本文成功制备了单层二硫化钼修饰的Cu_7S_4-Au纳米结构(Cu_7S_4-Au@S-MoS_2), 通过阳极溶出伏安法实现了对汞的灵敏选择性分析检测. 基于超小(<10 nm)单层MoS_2丰富的活性位点及金对汞的良好亲和性, 该方法灵敏度高(检出限为190 nmol L^{-1})、选择性好(常见Cd^{2+}、Pb^{2+}、Cu^{2+}等均无干扰), 并成功用于实际样品中汞的灵敏分析. 研究发现Cu_7S_4-Au与Cu_7S_4@S-MoS_2对Hg(II) (1.0 μmol L^{-1})无响应, 而多层MoS_2修饰的Cu_7S_4-Au(Cu_7S_4-Au@M-MoS_2)对Hg(II) (1.0 μmol L^{-1}) 有弱响应, 结果表明超小单层MoS_2丰富的活性位点及金对汞的良好亲和性对分析检测起到了协同催化作用.